Proceedings of the 10th World Congress on Mechanical, Chemical, and Material Engineering (MCM'24)
Barcelona, Spain –August 22-24, 2024
Paper No. HTFF 262
DOI: 10.11159/htff24.262

Insights into Pool Boiling Heat Transfer on Microchannel Surfaces

Md Motiur Rahaman[1], Praveen Dhanalakota[1], Pallab Sinha Mahapatra[1], Sarit K. Das[1], and Arvind Pattamatta[1, *]
[1]Department of Mechanical Engineering, Indian Institute of Technology Madras, Chennai-600036, India
*****Corresponding Author: arvindp@iitm.ac.in

Abstract –
The present study investigates the pool boiling heat transfer on two parallel microchannels of square cross-section with hydraulic diameters of 0.5 mm and 0.2 mm. Infrared (IR) thermography and thin-foil heating are employed to measure the temperature and heat flux fields, while a high-speed camera captures bubble dynamics. The combination of thermal imaging and high-speed videography offers comprehensive insights into the microscale boiling processes, aiding the optimization of microchannel heat exchangers in high-performance electronic devices. Understanding these dynamics is essential for designing cooling systems that manage increased heat loads, ensuring reliability and efficiency. This research highlights the critical role of channel geometry in enhancing pool boiling heat transfer performance and advancing thermal management in electronics. It is observed that the microchannel surfaces significantly improve pool boiling heat transfer compared to a flat surface. Surface area increase is the dominant heat transfer enhancement factor compared to separate liquid-vapor pathways for microchannels in pool boiling. In addition, it is also observed that pool boiling heat transfer enhancement depends not only on the surface area increase but also on the channel depth. For similar surface area augmentation factors, the channels with larger depths performed better. The deeper channels prevent vapor film formation and make bubbles depart at low diameters, thereby improving heat transfer and critical heat flux. Further studies on pool boiling over various deeper microchannel and minichannel surfaces with different working fluids are recommended to get more insights.

Keywords**:** Pool Boiling, Infrared Thermography, Microchannels, Heat Transfer, Field Measurements, Bubble Dynamics

1. Introduction

In electronics cooling, effective thermal management is critical to ensure the reliable operation and longevity of electronic devices and systems. As electronic components continue to shrink in size and increase power density, the demand for efficient cooling solutions becomes ever more demanding. Among the various thermal management techniques, pool boiling is a promising approach for dissipating heat from electronic chips. Pool boiling, characterized by the formation and departure of vapor bubbles on a heated surface immersed in a liquid, offers several advantages for electronics cooling applications. Its passive nature and high heat transfer coefficients through liquid-vapor phase change make it an attractive choice for efficiently removing heat from compact, densely packed electronic devices. Moreover, pool boiling can accommodate fluctuating heat loads and operate under varying environmental conditions, providing versatility and robustness in cooling electronic components.

The pursuit of adequate pool boiling-based cooling solutions for electronics has spurred extensive research into understanding the underlying mechanisms and optimizing heat transfer performance. Fundamental studies have elucidated the key factors influencing pool boiling heat transfer, including surface properties, fluid characteristics [1-2], operating conditions, and geometric configurations[3-5]. Insights gained from these investigations have paved the way for developing innovative heat transfer enhancement techniques tailored to meet the specific requirements of electronic cooling. The conventional approaches, which utilize thermocouples and high-speed boiling visualization [6-8], have several drawbacks. For instance, thermocouples can only measure temperature at specific points on the boiling surface, thus preventing the acquisition of information regarding temperature distribution around a nucleation site.

A significant research gap exists in measuring heat flux and temperature fields using infrared thermography with parallel microchannels during saturated pool boiling. However, optimizing their design requires a detailed understanding of the dynamic interactions between thermal and fluid phenomena. This study examines different microchannel surfaces to understand how geometry affects heat transfer and temperature fields. Additionally, bubble dynamics are captured using a high-speed camera. Combining data from IR thermography and high-speed cameras will improve our understanding of the

impact of microchannel geometry on heat transfer and boiling behavior, leading to better designs for thermal management systems.

2. Experimental Methodology

Temperature and heat flux measurements during pool boiling are obtained using infrared thermography, a high-speed optical camera, and thin-foil heating. The experimental setup comprises a boiling chamber, pressure transducer, condenser, thin foil heater, auxiliary heater, and DC power supply, which is shown in Figure 1. The boiling vessel, made of polycarbonate plates sealed with silicone gaskets, is filled with de-ionized water (Merck). The test section is mounted on a Teflon bottom plate with a 10 × 10 mm² aperture for IR visualization and secured by a stainless-steel plate with a matching opening for direct water exposure. The thin foil heater, made of 30 µm thick stainless steel (SS-304), is heated by a DC current from a TDK-Lambda power supply, monitored by a Fluke 362 clamp meter. A 0.25 mm JB-Weld layer, providing electrical insulation and good thermal conductivity (7.47 W/mK), separates the heater foil from the sample. The micro thermocouples' location in the microchannel samples is shown in Figure 2. K-type micro thermocouples (Omega), with 0.2 mm beads, are embedded in the boiling samples to verify infrared thermography and conduction simulation results. A reflux condenser, connected to a Subzero Instruments chiller, stabilizes pressure by condensing vapor. An auxiliary cartridge heater, controlled by a PID controller, keeps the water pool saturated at atmospheric pressure. Internal pressure is monitored using a Wika Instruments pressure transducer, and a keysight data logger records data from the thermocouples and pressure transducer.

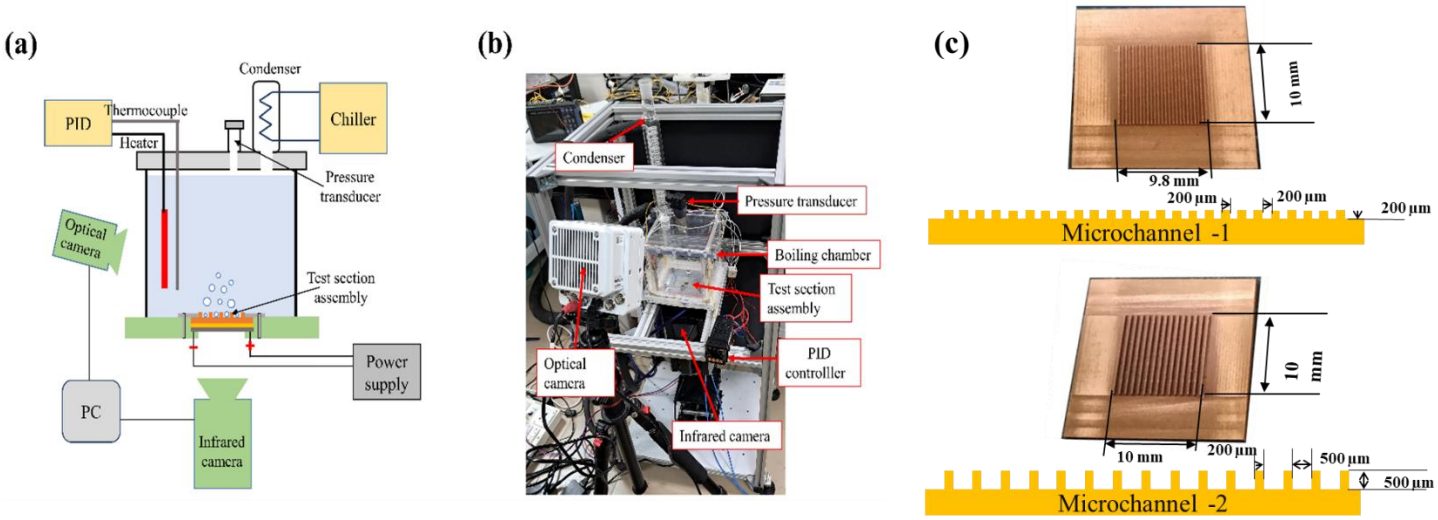

Figure 1: (a) Schematic of the experimental setup. (b) Actual experimental setup. (c) Copper Microchannels.

The experimental procedure begins by submerging test samples in a 15 wt% nitric acid solution for 15 minutes, then rinsing with de-ionized water to remove the atmospheric oxide layer. De-ionized water in the boiling chamber is degassed by boiling at 100°C for two hours with an auxiliary heater, venting non-condensable gases through a reflux condenser. A PID-controlled heater maintains the water's saturation temperature, while vapor condensation is regulated to keep the internal pressure at atmospheric levels, monitored by a pressure transducer. The foil, placed on busbars and heated with DC current, has its bottom surface coated with matte black high-temperature paint (emissivity 0.92, thickness 10 µm, thermal conductivity 1.45 W/mK) to enhance emissivity. A high-speed infrared camera (FLIR X6900sc MWIR) with a microscopic lens captures thermal images at 1000 Hz with a 25 µm resolution, covering a 1 × 1 cm² area (400 × 400 pixels) on the foil. This process ensures accurate temperature and heat flux measurements during the pool boiling experiments.

The boiling surface's thermal performance is investigated under steady-state conditions. Figure 3 (a) depicts the definition of the steady-state condition. The steady-state condition is a temperature change of less than 1 ℃ over 15 minutes in the micro thermocouples embedded in the boiling sample. Once this condition is met, the infrared camera captures the

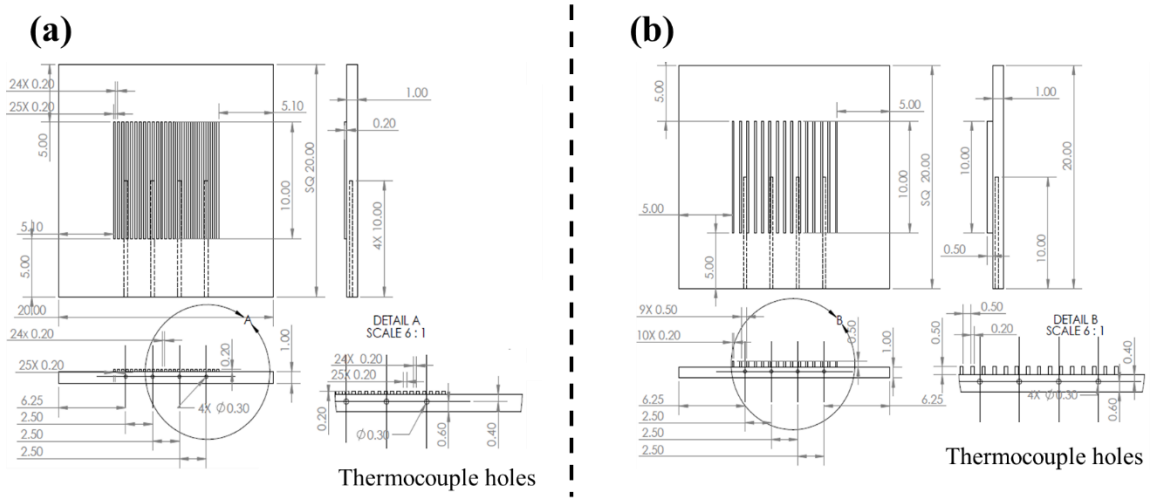

Figure 2: Micro-thermocouple locations on (a) Microchannel-1. (b) Microchannel-2.

temperature of the heater foil for 15 seconds at a rate of 1000 Hz. Figure 3 (b) shows the spatial average temperature of the heater foil surface during these 15 seconds, demonstrating no significant variation in the spatial average temperature of the heater foil surface. The steady-state temperature field of the heater foil is computed by averaging the data from 15,000 frames captured over 15 seconds.

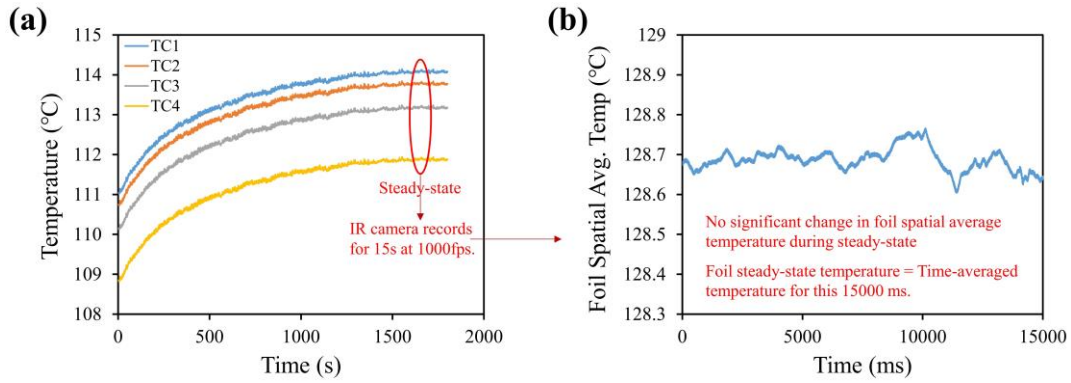

Figure 3: (a) Definition of steady-state condition. (b) Spatial average temperature of the heater foil surface.

3. Data Reduction

The experimental methodology is outlined in Figure 4. The infrared camera is initially calibrated to the required integration time and frame rate. Subsequently, the temperature data recorded by the infrared camera is smoothed to remove noise. The second step involves extracting the heat flux field by conducting a pixel-wise energy balance on the heater foil's temperature field [9]. The illustration of energy balance at a pixel element for the heat flux field is illustrated in Figure 5. The application of energy balance to the pixel element gives Equation 1, and the boiling heat flux field can be calculated.

The third step in the experimental methodology involves conducting a 3D steady-state conduction simulation to estimate the temperature distribution on the boiling surface. This simulation is carried out using the commercial software Ansys Fluent 20R1. The boundary conditions for the simulation are depicted in Figure 6. Specifically, the temperature profile obtained from the infrared camera is applied to the bottom surface of the stainless steel (SS) heater foil, while the heat flux profile obtained from the energy balance on the heater foil is applied to the copper boiling surface, assuming steady-state conditions. All other surfaces are assumed to be adiabatic. To ensure accuracy, the mesh is generated with 400 × 400 face cell centroids on both the heater foil surface and the boiling surface, matching the resolution of the temperature and heat flux fields. The mesh consists of 8.16 million cells and is finer than that used in the grid independence study. This finer mesh

prevents interpolation errors in Fluent's treatment of temperature and heat flux profiles provided as boundary conditions. In the fourth and final step, the temperatures obtained from the conduction simulation are compared with readings from micro thermocouples to verify their accuracy. The field measurements are deemed reliable and accurate when a strong agreement exists between the temperatures derived from the conduction simulation and those recorded by the micro thermocouples.

$$Q_{stored} = Q_{gen} + Q_{cond} - Q_{rad} - Q_{conv} - Q_{boil} \quad (1)$$

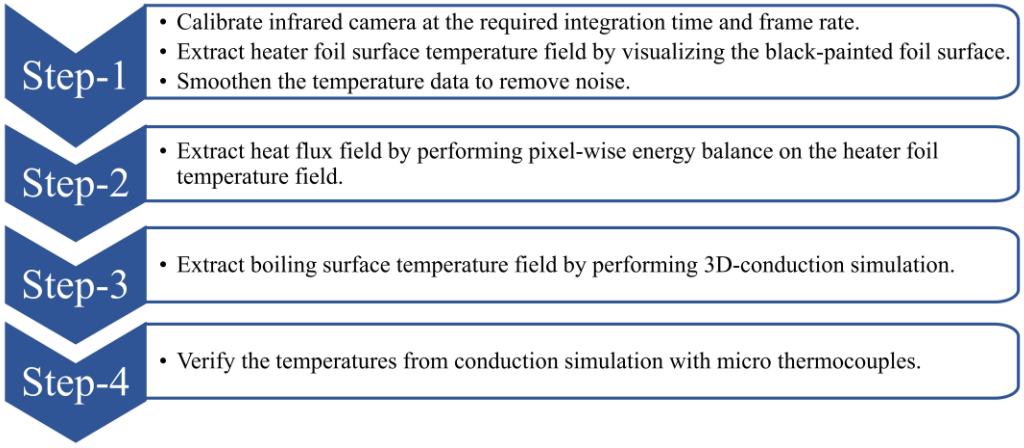

Figure 4: Outline of the experimental methodology for field measurements.

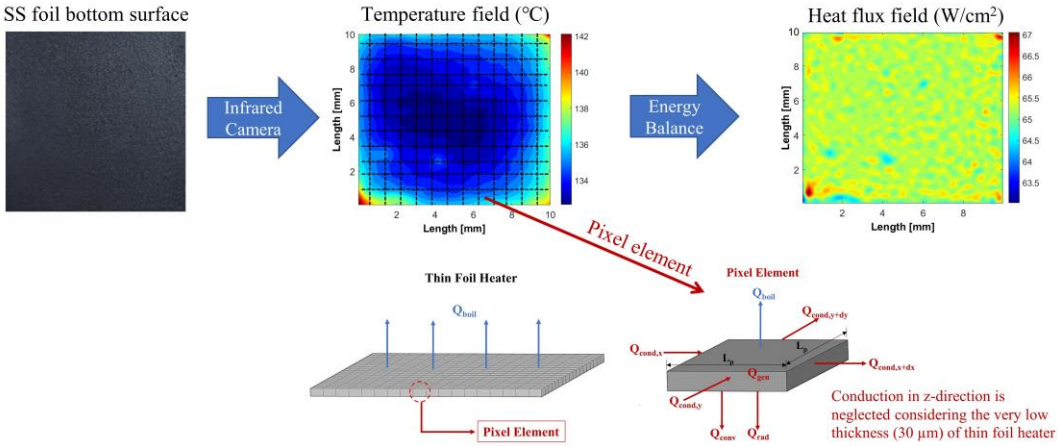

Figure 5: Illustration of energy balance at a pixel element for heat flux field.

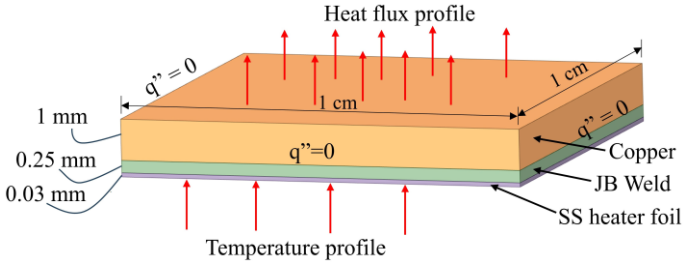

Figure 6: Boundary conditions for 3D steady-state conduction simulation.

3. Results and Discussion

3.1. Field measurements of temperature and heat flux:

Applying energy balance to the heater foil surface determines the heat flux field, while conduction simulation reveals the temperature field of the boiling surface. Figure 7 provides the temperature and heat flux field measurements for the flat surface, microchannel-1, and microchannel-2. Specifically, Figures 7 (a1), (b1), (c1) and, (a2), (b2), (c2) display the measurements for heat fluxes of 8 W/cm² and 85 W/cm², respectively. The same procedure was applied to 24, 44, and 65 W/cm² heat fluxes. However, the heat flux could not be increased beyond 85 W/cm² as the JB-Weld could not withstand it, resulting in the loss of contact between the heater foil and the boiling sample. The temperature fields of the heater foil are compared among flat surface, microchannel-1, and microchannel-2, shown in Figure 8 (a1) and (a2) for heat fluxes of 8 W/cm² and 85 W/cm², respectively. It is seen that the temperature of heater foil is lower for the microchannels compared to the flat surface. The heater surface temperature reaches its lowest point in microchannel-2. Figure 8 (b1) and (b2) compare the boiling surface temperature fields for the flat surface, microchannel-1, and microchannel-2. The boiling surface temperatures are lower for microchannels compared to the flat surface. The boiling surface temperature is the lowest for microchannel-2.

Figure 9 compares the steady-state temperatures derived from conduction simulation and temperature measured by micro thermocouples at identical locations. The temperatures obtained from conduction simulation and micro thermocouples fall within the uncertainty limits, indicating a strong agreement between the two methods for all heat fluxes. The good agreement between them verifies that the results from field measurements are reliable and correct. Figure 10 compares the steady-state pool boiling curves for flat surface obtained from field measurements with point measurements available in the literature. The temperature and heat flux in the pool boiling curve from field measurements represents the spatial average value of temperature and heat flux fields. The temperatures and heat fluxes obtained from both field measurements and point measurements fall within the uncertainty limits, indicating a strong agreement. This consistency between the pool boiling curves derived from field measurements and point measurements further confirms the reliability and accuracy of the results obtained from field measurements.

Figure 11(a) shows the boiling curves for all tested surfaces based on the projected area of the heater foil or the base area of the boiling surface (1 cm²). The pool boiling curve is shifted to the left side for microchannels compared to a flat surface. This implies that the heat flux increases at the same wall superheat (T_w). This indicates a significant improvement in heat transfer due to modification of the surface structure compared to a flat surface. The heat transfer coefficient of the tested samples based on the projected area or base area is shown in Figure 11(b). The heat transfer coefficient of flat surface, microchannel-1, and microchannel -2 increased from 1.77 to 4.99 W/cm^{2}K, 2.68 to 5.68 W/cm^{2}K, and 4.16 to 6.15 W/cm^{2}K, respectively, when the heat flux increased from 8 W/cm² to 85 W/cm². The heat transfer coefficient is enhanced by 13.35 – 59.33% and 20.29 – 155.19% for microchannel-1 and microchannel-2 than a flat surface. Microchannel-2 exhibits the highest performance, while the flat surface shows the lowest. Microchannel -1 performs better than the flat surface but not as well as Microchannel -2.

The superior performance of the microchannels over the flat surface can be due to the following reasons. In microchannels, the liquid inside a channel is heated from three sides, allowing nucleation at lower superheat levels. Bubble nucleation occurs at the channel base because of the shorter distance from the heater foil and the entrapment of superheated liquid within the channels. The formation of bubbles inside the channels establishes separate liquid-vapor pathways, accelerating bubble removal and enhancing the rewetting of the boiling surface. On the other hand, the augmentation of the total wetted surface area due to microchannel formation can amplify the heat transfer during boiling compared to a flat surface. This rise in heat transfer is caused by an increase in surface area with the formation of microchannels, which resembles a fin effect. To find out the dominant heat transfer enhancement factor, pool boiling curves and heat transfer coefficients based on the total wetted area are plotted in Figure 12. It can be seen that the pool boiling curves and heat transfer coefficients of microchannels are falling on or below that of a flat surface. This indicates that the increase in surface area is the dominant heat transfer enhancement factor.

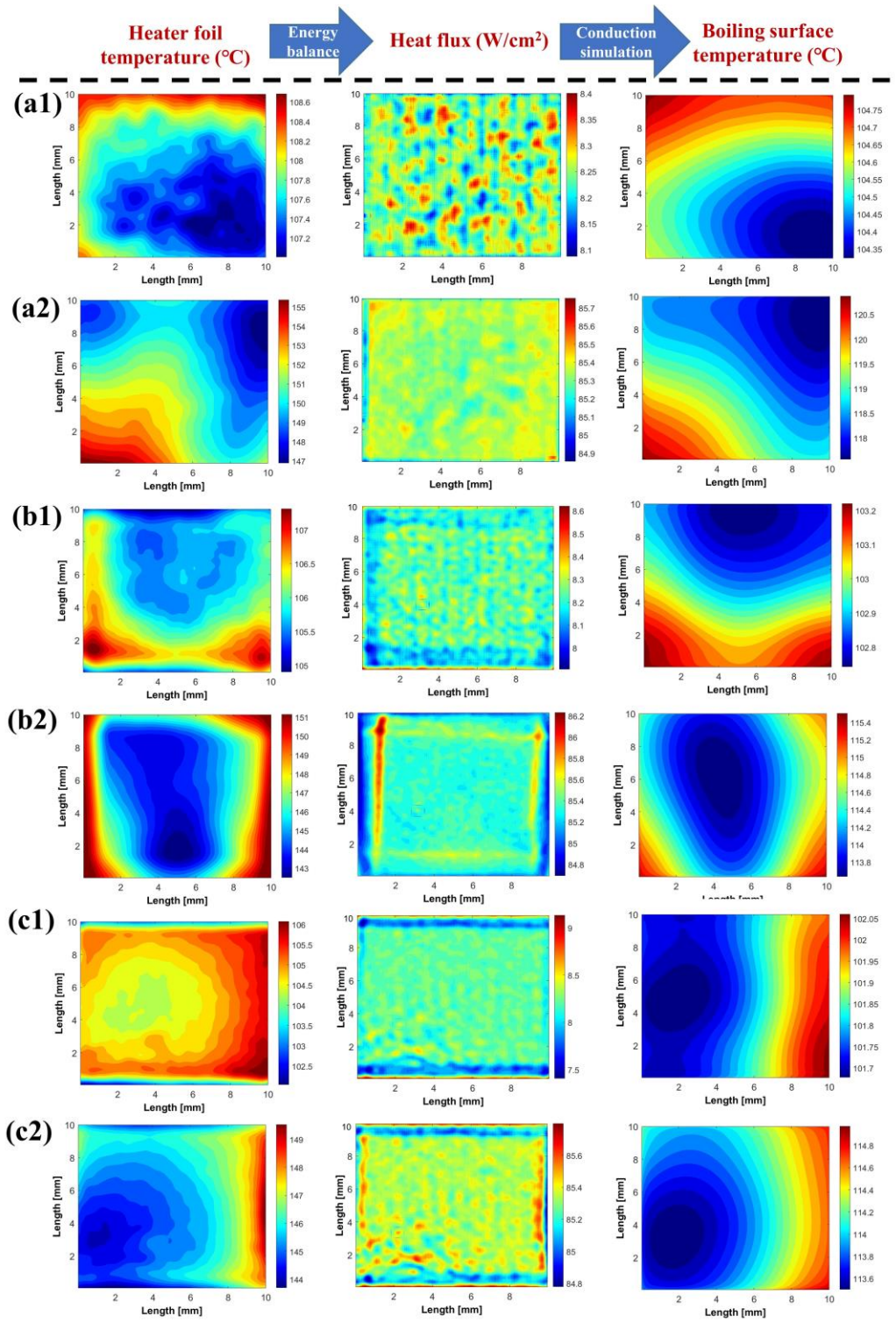

Figure 7: Field measurements of temperature and heat flux: Flat surface: (a1) 8 and (a2) 85 W/cm^2. Microchannel-1:(b1) 8 and (b2) 85 W/cm^2. Microchannel-2: (c1) 8 and (c2) 85 W/cm^2.

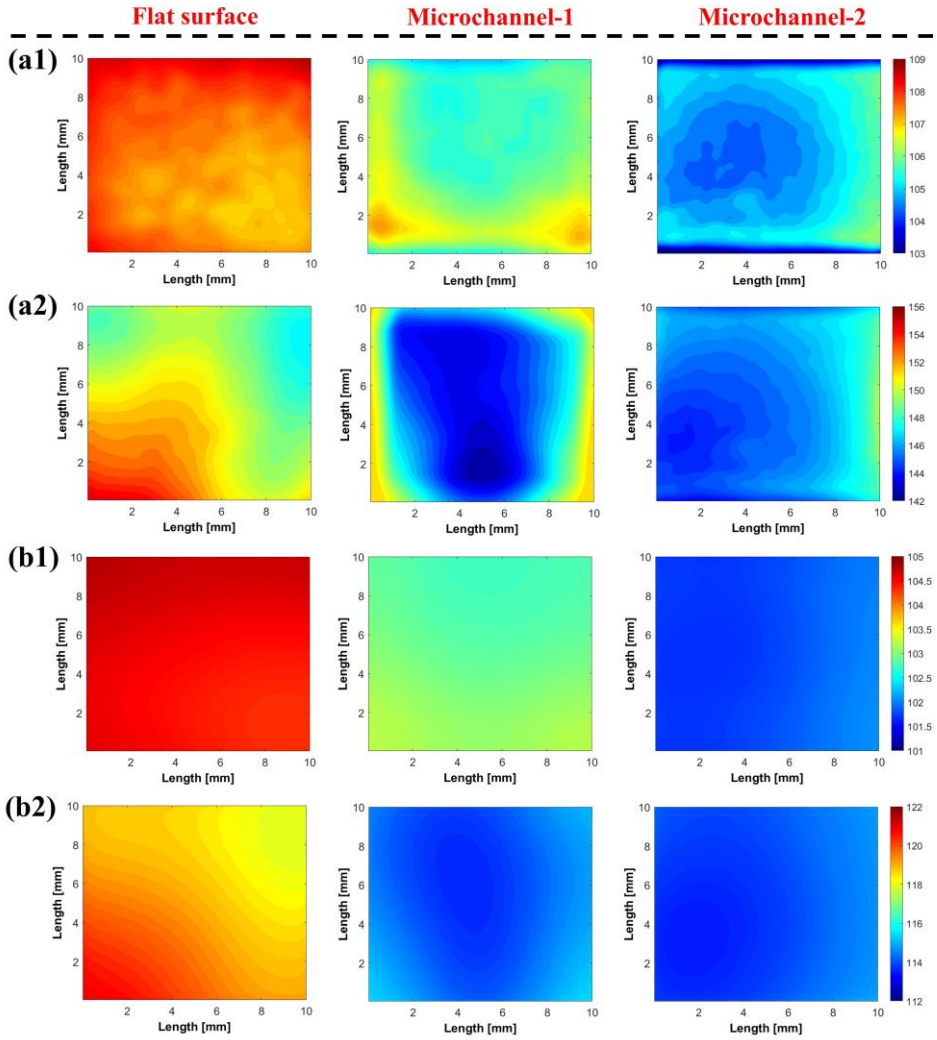

Figure 8: Comparison of heater foil temperature field: (a1) 8 W/cm^2 and (a2) 85 W/cm^2. Comparison of boiling surface temperature field: (b1) 8 W/cm^2 and (b2) 85 W/cm^2

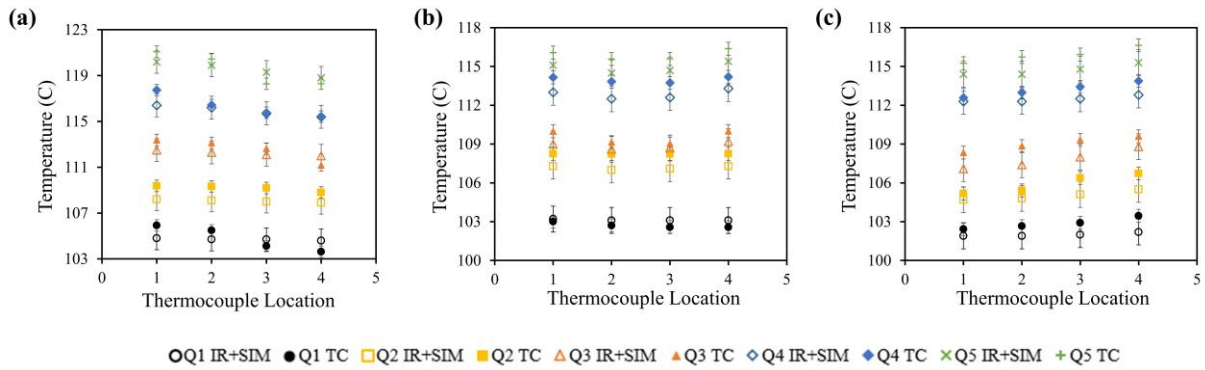

Figure 9: Verification of temperatures from Infrared thermography and conduction simulation (IR+SIM) with micro-thermocouples (TC) during field measurements at different heat fluxes (Q1, Q2, Q3, Q4, and Q5 are 8, 24, 44, 65, and 85 W/cm^2, respectively): (a) Flat surface. (b) Microchannel-1. (c) Microchannel-2.

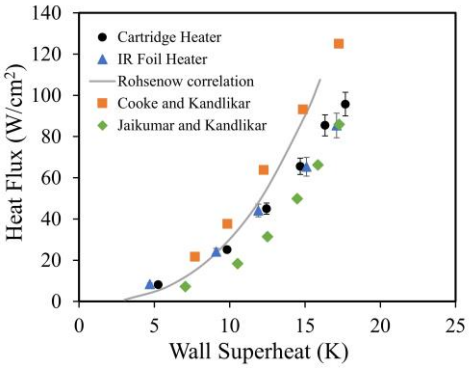

Figure 10: Verification or comparison of pool boiling curves for flat surface from field measurements (foil heater and infrared thermography with conduction simulation) with standard cartridge heater and literature.

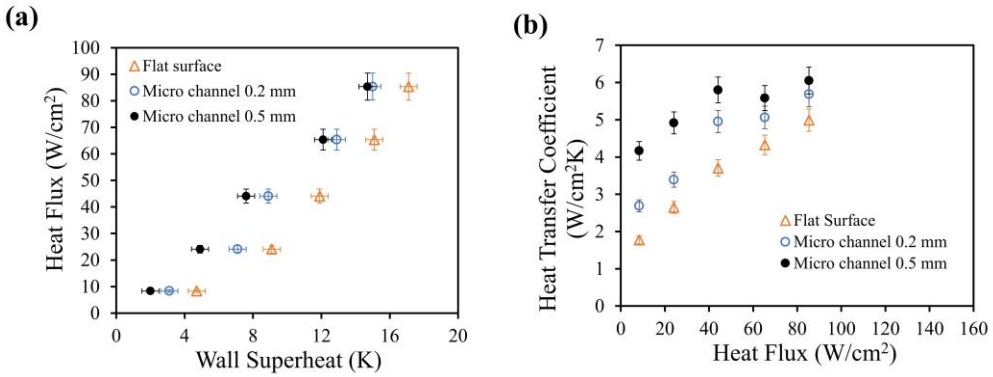

Figure 11: (a) Pool boiling curves and (b) Heat transfer coefficients based on projected or base area.

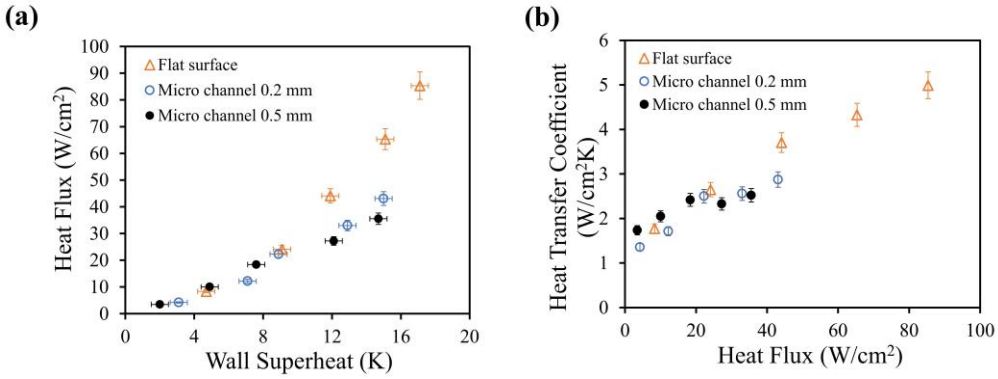

Figure 12: (a) Pool boiling curves and (b) Heat transfer coefficients based on total wetted area.

3.2. Comparison between microchannel and minichannel surfaces:

The pool boiling phenomena on the microchannel surface are compared with that of the minichannel surface, which has a similar surface area, to get insights into the effect of channel depth on pool boiling. The geometrical parameters of the test samples are listed in Table 1. The surface area augmentation factor is the ratio of the total wetted area of the boiling surface that is exposed to the liquid pool to the projected area of the heater foil or base area of the boiling surface (1 cm^2). The total wetted area depends on the channel width, channel depth, fin width, and number of channels.

Table 1: Geometrical Parameters of Microchannel and Minichannel Surfaces.

Parameter	**Micro channel 0.5 mm**	**Mini channel 2 mm**
Channel depth	0.5 mm	2 mm
Channel width	0.5 mm	2 mm
Fin width	0.2 mm	1 mm
No. of channels	14	3
Surface area augmentation factor	2.4	2.2

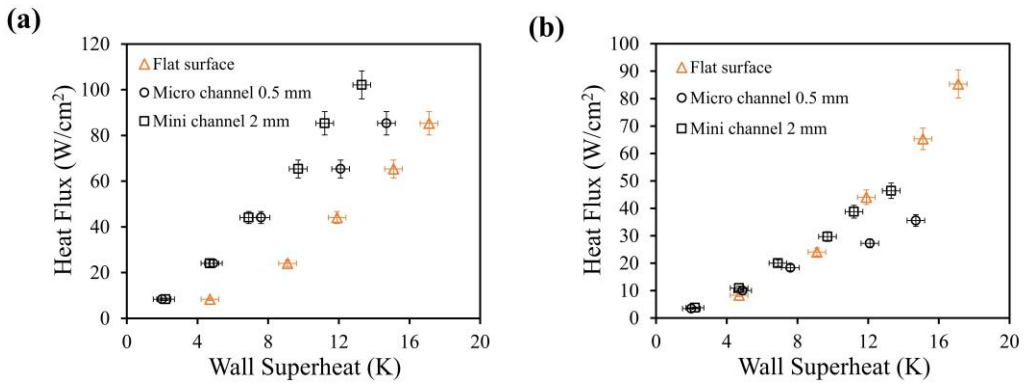

Figure 13: Comparison of pool boiling curves between microchannel and minichannel based on (a) Projected or base area. (b) Total wetted area.

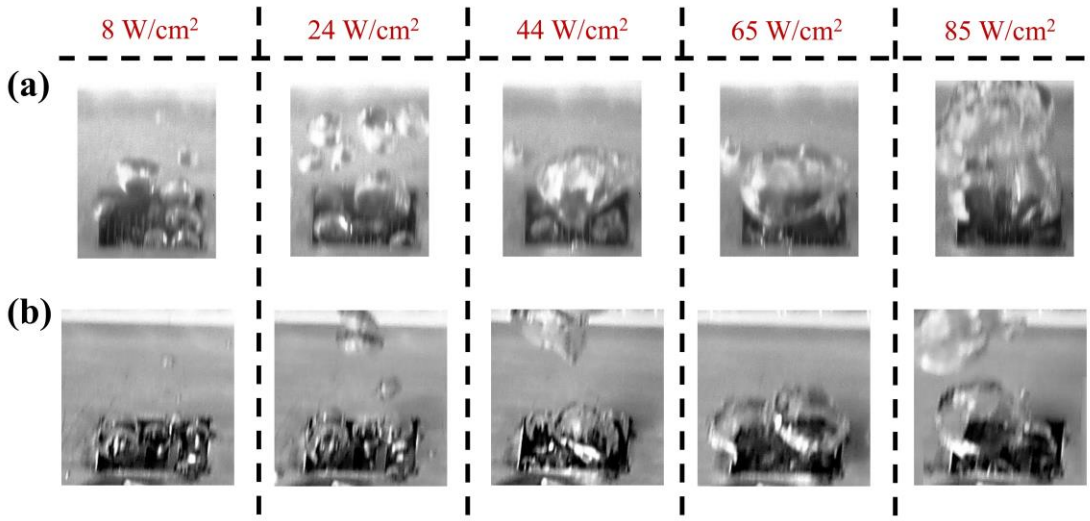

Figure 14: Comparison of bubble dynamics between (a) Microchannel 0.5 mm and (b) Minichannel 2mm.

Figure 13 (a) represents the pool boiling curves based on the projected or base area for all the samples. The results show that heat transfer is higher with microchannel and minichannel surfaces compared to flat surface. The pool boiling curves based on the total wetted area are plotted in Figure 13 (b) to find out the dominant enhancement factor, whether it is surface area increase or separate liquid-vapor pathways. It can be seen that the pool boiling curves of micro and mini channels based on the total wetted area fall on or below that of a flat surface. This implies that the increase in surface area is the dominant enhancement factor for both microchannel and minichannel surfaces in pool boiling. It is also observed that the minichannel-2mm performs better than microchannel-0.5mm despite having slightly less or similar total wetted area or surface area augmentation factor. The better performance of minichannel-2mm compared to microchannel-0.5mm is due to the larger

channel depth. It can be evident from Figure 14 that compares bubble dynamics of microchannel and minichannel. It can be seen from Figure 14 that the bubble departure diameters are less for the minichannel (Figure 14b) compared to the microchannel (Figure 14a). The deeper channels of the minichannel surface prevent vapor film formation and make bubbles depart at low diameters, thereby improving heat transfer and critical heat flux compared to the microchannel surface.

The present research work reveals that pool boiling heat transfer enhancement depends not only on the surface area increase but also on the channel depth. For similar surface area augmentation factors, the channels with larger depth performed better. In addition, it is observed that the increase in surface area is the dominant heat transfer enhancement factor compared to separate liquid-vapor pathways for microchannels in pool boiling. However, Cooke and Kandlikar[5] reported that separate liquid-vapor pathways as the dominant enhancement factor compared to surface area increase for microchannels in pool boiling with water. Moreover, the research work by Kalani and Kandlikar [8] from the same group reported that the surface area increase is the dominant enhancement factor compared to separate liquid-vapor pathways for microchannels in pool boiling with FC-87. In addition, they observed that the finned minichannel surface with a larger channel depth performed better than the microchannels. The results from the present research work are in accordance with that of Kalani and Kandlikar [8] despite having a difference in working fluid. Further studies on pool boiling over various deeper microchannel and minichannel surfaces with different working fluids are recommended to get more insights.

4. Conclusions

The present work experimentally investigates pool boiling heat transfer on microchannel surfaces through field measurements of temperature and heat flux using infrared thermography and thin-foil heating. The following conclusions are obtained.

- Microchannel surfaces significantly improved pool boiling heat transfer compared to a flat surface.
- It is observed that the increase in surface area is the dominant heat transfer enhancement factor compared to separate liquid-vapor pathways for microchannels in pool boiling.
- Pool boiling heat transfer enhancement depends not only on the increase in surface area but also on the channel depth. For similar surface area augmentation factors, the channels with larger depths performed better.
- Further studies on pool boiling over various deeper microchannel and minichannel surfaces with different working fluids are recommended to get more insights.

Acknowledgements

The first author acknowledges Prime Minister Research Fellowship (PMRF) from the Indian government.

References

[1] U. Sajjad, A. Sadeghianjahromi, H. M. Ali, and C. C. Wang, “Enhanced pool boiling of dielectric and highly wetting liquids - a review on enhancement mechanisms,” *International Communications in Heat and Mass Transfer*, vol. 119, Dec. 2020, doi: 10.1016/j.icheatmasstransfer.2020.104950.

[2] E. Wagner and P. Stephan, “High-resolution measurements at nucleate boiling of pure FC-84 and FC-3284 and its binary mixtures,” *J. Heat Transfer*, vol. 131, no. 12, pp. 1–12, Dec. 2009, doi: 10.1115/1.3220143.

[3] M. Piasecka, “Heat transfer research on enhanced heating surfaces in flow boiling in a minichannel and pool boiling,” *Ann Nuclear Energy*, vol. 73, pp. 282–293, 2014, doi: 10.1016/j.anucene.2014.06.041.

[4] A. Walunj and A. Sathyabhama, “Comparative study of pool boiling heat transfer from various microchannel geometries,” *Applied Thermal Eng*, vol. 128, pp. 672–683, 2018, doi: 10.1016/j.applthermaleng.2017.08.157.

[5] D. Cooke and S. G. Kandlikar, “Effect of open microchannel geometry on pool boiling enhancement,” *Int J Heat Mass Transfer*, vol. 55, no. 4, pp. 1004–1013, Jan. 2012, doi: 10.1016/j.ijheatmasstransfer.2011.10.010.

[6] R. Kaniowski and R. Pastuszko, “Pool boiling visualization on open microchannel surfaces.”

[7] A. M. Gheitaghy, A. Samimi, and H. Saffari, “Surface structuring with inclined minichannels for pool boiling improvement,” *Applied Thermal Eng*, vol. 126, pp. 892–902, Nov. 2017, doi: 10.1016/j.applthermaleng.2017.07.200.

[8] A. Kalani and S. G. Kandlikar, “Pool boiling of fc-87 over microchannel surfaces at atmospheric pressure,” In ASME International Mechanical Engineering Congress and Exposition, vol. 45233, pp. 2051-2057. American Society of Mechanical Engineers, 2012

[9] G. Guggilla, R. Narayanaswamy, and A. Pattamatta, “An experimental investigation into the spread and heat transfer dynamics of a train of two concentric impinging droplets over a heated surface,” *Exp Thermal Fluid Sci*, vol. 110, Jan. 2020, doi: 10.1016/j.expthermflusci.2019.109916.